Chemical Engineering Journal 253 (2014) 264–273

Contents lists available at ScienceDirect

Chemical Engineering Journal

journal homepage: www.elsevier.com/locate/cej

Enhanced adsorption of hydrogen sulfide and regeneration ability on the composites of zinc oxide with reduced graphite oxide

Hoon Sub Song [a,e], Moon Gyu Park [a], Wook Ahn [b], Sung Nam Lim [c], Kwang Bok Yi [d], Eric Croiset [a,*], Zhongwei Chen [a], Sung Chan Nam [e,*]

[a] Department of Chemical Engineering, University of Waterloo, 200 University Avenue West, Waterloo, Ontario N2L3G1, Canada
[b] Department of Materials Science & Engineering, Yonsei University, 50 Yonsei-ro, Seodaemun-Gu, Seoul 120-749, Republic of Korea
[c] Department of Chemical & Bimolecular Engineering, Korea Advanced Institute of Science and Technology, 291 Daehak-ro, Yuseong-gu, Daejeon 305-701, Republic of Korea
[d] Department of Chemical Engineering Education, Chungnam National University, 99 Daehak-ro, Yuseong-gu, Daejeon 305-764, Republic of Korea
[e] Greenhouse Gas Department, Korea Institute of Energy Research, 152 Gajeong-ro, Yuseong-gu, Daejeon 305-343, Republic of Korea

HIGHLIGHTS

- Reduced graphite oxide (rGO) promotes the H_2S adsorption efficiency of metal oxide.
- Oxygen functional groups on rGO affect the chemical state of zinc oxide.
- ZnO/rGO composite shows about 5 times higher H_2S adsorption capacity.
- ZnO/rGO composite shows stable regeneration efficiency over 8 cycles.

ARTICLE INFO

Article history:
Received 28 March 2014
Received in revised form 13 May 2014
Accepted 14 May 2014
Available online 22 May 2014

Keywords:
Hydrogen sulfide
Reduced graphite oxide
Zinc oxide
Adsorption
Regeneration

ABSTRACT

Interaction of oxygen-containing functional groups on reduced graphite oxide (rGO) surface and zinc oxide (ZnO) has been investigated; and critical functionalities of rGO for enhancing H_2S adsorption were studied. The abundant oxygen functional groups attached on the surface of rGO promoted the dispersion of nano-sized ZnO; then a higher surface area on the adsorbents was achieved. In addition, they prevented the aggregation of ZnO particles during regeneration at 600 °C. Beside those physical property changes, the presence of rGO modified the chemical properties of ZnO, as confirmed by XPS analysis. Due to those oxygen functional groups, the amount of zinc ions (Zn^{2+}) are placed at the oxygen vacant sites, not only in the Zn–O lattice on ZnO/rGO composite. It was determined that the amount of oxygen ions in the Zn–O lattice decreased; and loosely bonded oxygen ions near the Zn–O lattice and on the surface were generated. Therefore, it was found that the presence of rGO plays a critical role to provide appropriate conditions for H_2S adsorption, which was confirmed through the H_2S adsorption breakthrough and regeneration tests. The ZnO/rGO composite showed about fivefold that of pure ZnO. The capacity after 1st regeneration for ZnO/rGO decreased by about 57% but then was maintained constant over 8 recycles while that on ZnO decreased dramatically to reach nearly zero capacity after 5 cycles.

1. Introduction

Hydrogen sulfide (H_2S) is one of the most common sulfur components and is considered as an undesirable component in most industrial applications since sulfur impurities rapidly deactivate or poison catalysts, which are widely used in the chemical or petrochemical industries [1]. Therefore, the removal of sulfur-containing gases (i.e. SO_2, H_2S etc.) has become a critical issue. Various approaches to remove H_2S, such as sorption, catalysis or condensation, have been applied [2]. Among those approaches, different adsorbents, such as activated carbon, zeolites [3,4], modified alumina [5] or metal oxides [6,7], have been investigated. Zinc oxide (ZnO) has been widely used as an adsorbent for removal of H_2S from hot gas steams (in range of 500–800 °C) with the formation of zinc sulfide (ZnS) by the following reaction ($ZnO_{(s)} + H_2S_{(g)} \rightarrow ZnS_{(s)} + H_2O_{(g)}$) [8]. There is a critical drawback, however, to use ZnO for hot-gas H_2S removal process. Due to its thermal instability,

* Corresponding authors. Tel.: +1 519 888 4567x36472 (E. Croiset), +82 42 860 3645 (S.C. Nam).
E-mail addresses: ecroiset@uwaterloo.ca (E. Croiset), scnam@kier.re.kr (S.C. Nam).

http://dx.doi.org/10.1016/j.cej.2014.05.058
1385-8947/

the ZnO adsorbent has a risk of evaporating as volatile metallic zinc [9]. For lower temperature applications, the thermal stability is not an issue and ZnO can be converted to ZnS at even ambient condition [10]. To date, several studies have been conducted under moist and dry conditions [11] for H_2S adsorption. It has been proposed that water is critical since moisture is able to dissociates H_2S into HS^- and S^{2-}; and the dissociated H_2S ions are chemically adsorbed on the surface [12,3]. It was confirmed that the carboxylate groups on a composite significantly decreased after H_2S exposure [13]. Different mechanisms, however, govern the adsorption for dry condition since direct replacement of the dissociated HS^- ions with –OH groups on oxide particles are dominant for sulfide formation.

Graphite oxide (GO) has been widely studied as an adsorbent since it contains various oxygen functional groups, such as hydroxides, epoxides, and carboxylic groups on the surface of GO plane [14,15]. Those negatively charged oxygen functional groups, which are known to anchor positively charged metal ions (i.e. Zn^{2+} or Cu^{+}) through hydrogen bonds, can be controlled quantitatively by varying the reduction processes. Reduced graphite oxide (rGO) has thus received dramatic attentions as a substrate for metal oxide deposition [14–18]. Using those benefits, active researches regarding metal oxides (copper [12], zirconium [17] cobalt [13] or zinc [19,20]) with rGO composites for acid gas (i.e. H_2S, SO_2 or COS) adsorption processes have been extensively studied recently.

As discussed above, many studies for H_2S adsorption have been conducted using metal oxide attached on the rGO surface. However, in-depth investigation of the effects of those oxygen functional groups on the metal oxide chemical states has not been studied. Therefore, in this study, the critical functionalities of those oxygen functional groups for H_2S adsorption were studied by investigating the change of the chemical status of metal oxides attached on rGO. In addition, from a practical point of view, regeneration of the sorbent is critical and this study also investigates the regenerability of the developed composite ZnO/rGO sorbent.

2. Experimental

2.1. Synthesis of graphite oxide

The synthesis of GO was based on our previous work [21]. GO was synthesized using a mixture of 360 mL of sulfuric acid (Sigma–Aldrich, ACS reagent, 95.0–98.0%) and 40 mL of phosphoric acid (Sigma–Aldrich, ACS reagent, ⩾85 wt.% in H_2O), and 3.0 g of graphite powder (Sigma–Aldrich, <45 μm, ⩾99.99%). This mixture was placed in an ice bath. When the temperature reached below 5 °C, 18.0 g of $KMnO_4$ (Samchun Chemical, 99.3%) was added slowly. The mixture was stirred for 1 h and then maintained at isothermal conditions at 50 °C for 18 h. The system was then cooled to room temperature naturally. The mixture was then placed in an ice bath again; and 400 mL of de-ionized water and 15 mL of 30% H_2O_2 (OCI Company Ltd., 30 wt.% in H_2O) were added gradually. The mixture turned then bright yellow and generated copious bubbles. The mixture was stirred for 1 h and then centrifuged at 3500 rpm for 3 min. The remaining solid paste was washed with a mixture of 100 mL of de-ionized water and 100 mL of 30% HCl (Sigma–Aldrich, ACS reagent, 37%) twice. The product was then rinsed twice again with 200 mL of de-ionized water. After the washing steps, the paste was freeze- and vacuum-dried overnight.

2.2. Synthesis of ZnO/rGO composites

400 mg of GO was dissolved in 200 mL of ethylene glycol (Sigma–Aldrich, ReagentPlus®, ⩾99%) and 100 mL of 0.1 M aqueous NaOH (Sigma–Aldrich, ACS reagent, ⩾97.0%) solution; then underwent ultra-sonication for 30 min. 0.07 M aqueous zinc and copper acetate (Sigma–Aldrich, ACS reagent, ⩾98%) solutions were prepared. Then, 100 mL of 0.07 M Zinc acetate solution was prepared and mixed with the GO solution; then sonicated for another 30 min. 300 μL of hydrazine solution (Sigma–Aldrich, 35 wt.% in H_2O) was added before the reduction process. The Zn/GO mixture was reduced by microwave irradiation for 3 min (1 min irradiation with 1 min break, 3 times). After cooling down, the mixture was filtered and washed with DI-water three times using centrifuge. Finally, the paste was freeze- and vacuum-dried overnight.

2.3. H_2S adsorption breakthrough and regeneration tests

Dynamic breakthrough tests were conducted at 300 °C. 0.5 cm^3 of the adsorbents diluted with 1.0 cm^3 of Al_2O_3 (Sigma–Aldrich, ~150 mesh) for a total of 1.5 cm^3 of bed were packed into a quartz tube (internal diameter 10 mm). In a typical test, a flow of H_2S (5 mL/min, 3.01 vol% of H_2S balanced with N_2) was mixed with 195 mL/min of N_2 gas before passing through the adsorbent bed. The initial H_2S concentration was 750 ppm with a total flow rate of 200 mL/min. For regeneration, N_2 only was flowed through the spent adsorbent at 600 °C for 1 h. The product stream was further diluted with 1800 mL/min of N_2 before injection to the H_2S analyzer due to the limitation of the H_2S analyzer (Fluorescence H_2S Analyzer, Model 101E, Teledyne) which could accommodate H_2S concentration only up to 10 ppm. The experiments were carried out until the output H_2S concentration, after dilution, reached ~5 ppm. The experimental breakthrough time was determined when the outlet H_2S concentration, after dilution, reaches 0.1 ppm. The amount of sulfur adsorbed per gram of adsorbent was calculated by Eq. (1):

$$\frac{\text{g of S}}{\text{g of Ads.}} = \frac{0.15\ \text{mL}\ H_2S}{\text{min}} \times \frac{1\ \text{mol}\ H_2S}{22{,}400\ \text{mL}\ H_2S} \times \frac{34.06\ \text{g S}}{1\ \text{mol}\ H_2S} \times \frac{32.06\ \text{g S}}{34.08\ \text{g}\ H_2S} \times t\left(\frac{\text{min}}{\text{g Ads.}}\right) \quad (1)$$

where t is the experimental breakthrough time (min/g of adsorbent).

2.4. Characterizations

X-ray diffraction (XRD, Rigaku, 40 kV/100 mA of X-ray, step size: 0.02°) was used for adsorbent characterization; 5–60° of 2θ range was measured. X-ray photoelectron spectroscopy (XPS, AXIS Ultra DLD, KRATOS Inc.) was used with mono chromatic A1 Ka (1486.6 eV) for X-ray source, 0.1 eV/step; and no surface treatment were used. Scanning electron microscopy (FE-SEM) images were obtained using a Hitachi S-4700 with an accelerating voltage of 5.0 kV.

3. Results and discussions

3.1. H_2S adsorption and regeneration ability

From an industrial point of view, regeneration of the adsorbent is critical. Multiple regeneration cycles for pure ZnO and ZnO/rGO composite were then studied. For all cases, identical sulfidation conditions (300 °C and 750 ppm H_2S) were used; and a temperature of 600 °C (in N_2 only) was used for regeneration. Fig. 1 shows the regeneration capacities (mg of sulfur adsorbed per gram of adsorbent) for pure ZnO (up to 5 cycles) and ZnO/rGO samples (up to 8 cycles).

The initial sulfur adsorption capacity for pure ZnO (31.7 mg S/g ads) corresponds to that reported in the literature [7,22]. The initial sulfur adsorption capacity for ZnO/rGO composite (172.6 mg S/g ads) was about 5.5 times higher than that from pure ZnO. After the first regeneration, the decrease in sulfur capacity for both

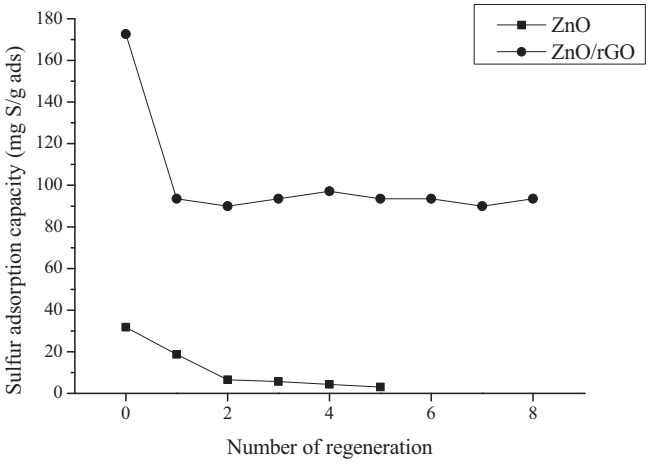

Fig. 1. H_2S adsorption capacities on ZnO and ZnO/rGO composite at 300 °C sulfidation with 600 °C regeneration in N_2.

samples were observed as 93.5 mg S/g ads for ZnO/rGO and 18.6 mg S/g ads for pure ZnO. It is clear that pure ZnO did not retain its sulfur adsorption capacity, which is nearly zero (3.1 mg S/g ads) after only 5 cycles. On the other hand, although the sulfur adsorption capacity decreases significantly after the first cycle for the ZnO/rGO composite (about 53% decrease from initial capacity), the adsorption capacity remains constant, at least over 8 cycles. This supports that the functionality of rGO as a substrate plays a critical role to enhance and maintain the sulfur adsorption capacity over multiple regeneration cycles. Therefore, deeper investigations on the effects of rGO as a substrate on the metal oxide, ZnO, are necessary in order to explains the H_2S adsorption capacity changes on pure ZnO and ZnO/rGO composite.

3.2. Physical property changes of ZnO/rGO composite

There are several aspects determining the adsorption capacity of the adsorbents. Surface area is an important factor affecting the adsorption capacity. The initial surface areas of ZnO and ZnO/rGO composite were 68.4 and 265.6 m^2/g, respectively. The higher surface area of ZnO/rGO composite was from the 2 dimensional (2D) rGO substrate since the rGO surface containing oxygen functional groups is able to disperse the nano-sized ZnO particles onto the surface. This increases the contact area of the active ZnO particles to the target molecules (i.e. HS^- and S^{2-}). After the first regeneration at 600 °C, the surface areas of ZnO and ZnO/rGO became 25.2 and 178.8 m^2/g, respectively. It can be observed that the surface area of ZnO dramatically decreased after the high temperature annealing. This phenomenon could explain the large drop in adsorption capacity after the first regeneration. After further regenerations, the surface area of ZnO was reduced to 15.2 m^2/g (after 5th cycles); but that of ZnO/rGO composite was maintained at 163.1 m^2/g (after 8th cycles). Clearly, the pattern for the change in surface area correlates somewhat that for the change in adsorption performance for both ZnO and ZnO/rGO.

Morphology changes over regeneration cycles were observed through SEM analysis (Fig. 2). For pure ZnO sample, the average initial particle size of ZnO was 939 nm. After 5 cycles, it was shown that the surface of ZnO was aggregated and cracks were observed (Fig. 2(b)). The cracks could be generated due to the multiple sulfidation-regeneration cycles of ZnO since the lattice structure of ZnO was partially destroyed over several cycles. On the other hand, the average particle size of ZnO in the ZnO/rGO composite was 62.7 nm after 8 cycles. This supports that the presence of rGO as a substrate distributes the nano-sized ZnO over the surface which, in turn, leads to the reduction of the particle size since it is been known that the oxygen functional groups on rGO surface are anchoring metal ions (Fig. 2(c) and (d)). After 8 cycles, the particle size of ZnO was not significantly changed and the overall shape of ZnO particles was maintained. This could explain the stable sulfur adsorption performance over 8 cycles.

The change in the crystal structure of ZnO/rGO over sulfidation-regeneration cycles is presented in Fig. 3. It is shown that the XRD patterns of pure ZnO at 2θ of 31.6, 34.3, 36.2, 47.4 and 56.4, corresponding to the crystal planes of (100), (002), (101), (102) and (110), respectively, were observed for the fresh ZnO/rGO composite (Fig. 3(a)). Those patterns are indexed to be wurtzite ZnO and matched with JCPDS 36-1451. No other characteristic peaks from

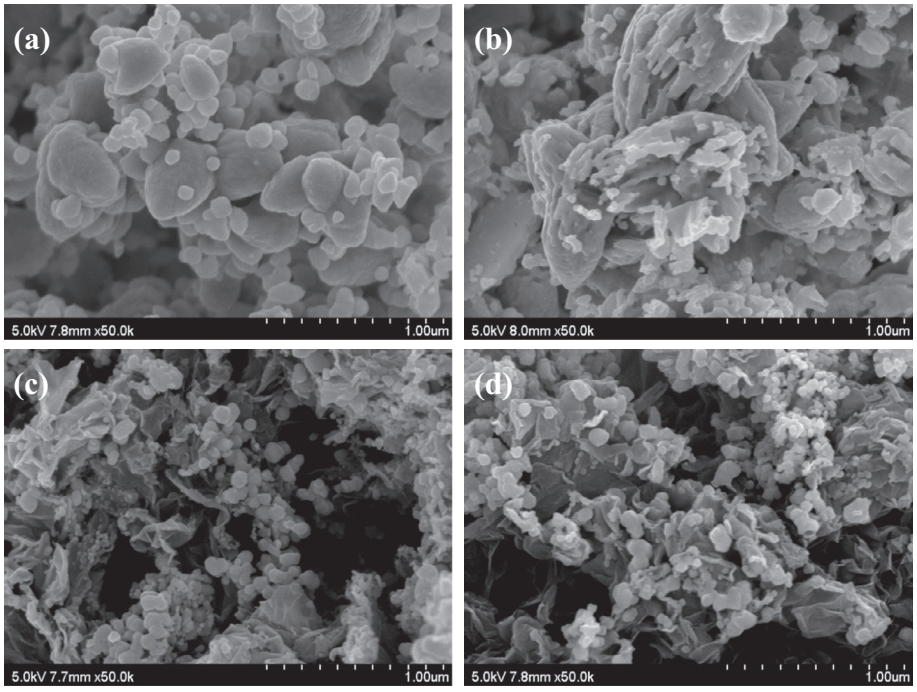

Fig. 2. Morphology changes during the regeneration cycles: (a) fresh ZnO, (b) ZnO after 5 cycles, (c) fresh ZnO/rGO and (d) ZnO/rGO after 8 cycles.

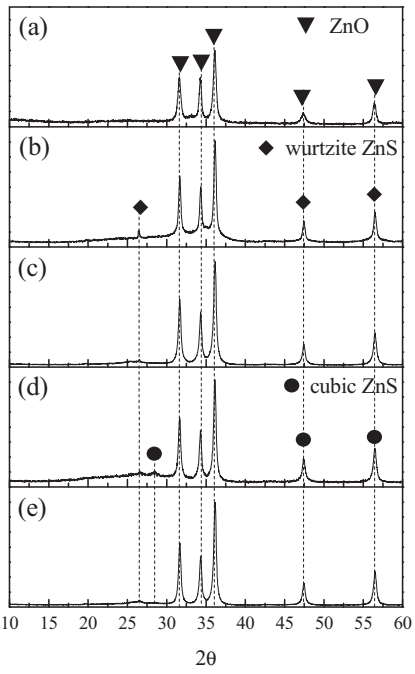

Fig. 3. XRD patterns for ZnO/rGO: (a) fresh, (b) after 1st sulfidation, (c) after 1st regeneration, (d) after 8th sulfidation and (e) after 8th regeneration.

impurities were detected. After the first H_2S adsorption (Fig. 3(b)), other characteristic peaks of wurtzite-structured ZnS were shown at 2θ of 26.5 (100), 47.5 (110) and 56.5 (112) (matched with JCPDS 75-1547) as well as peaks for pure ZnO simultaneously. It is suggested that the Zn–O (wurtzite) crystal structure was converted to Zn–S (wurtzite) from the first H_2S adsorption. However, after the first regeneration (Fig. 3(c)), the intensity of the (100) ZnS peak was lowered. This implies that the Zn–S structure was partially destroyed and the sulfur atoms were detached from the zinc atom during the regeneration process. After the 8th H_2S adsorption (Fig. 3(d)), other ZnS peaks were observed at 2θ of 28.43, 47.43 and 56.50; and those peaks were identified as cubic (or sphalerite) ZnS corresponding to (111), (220) and (311) planes, respectively (matched with JCPDS 77-2100). Like the first regeneration, after the 8th regeneration (Fig. 3(e)), the wurtzite and cubic structured ZnS peaks were weakened, but still present due to the limited regeneration efficiency. However, in general, the overall shape and location of the peaks were very similar during the multiple cycles. The results presented here suggest that the ZnO/rGO composite possesses a stable crystal structure of ZnO and ZnS over cycles; and it supports the stable H_2S adsorption efficiency over eight sulfidation-regeneration cycles.

3.3. Chemical property changes on ZnO/rGO composite

Beside the metal oxide dispersion effect, the change in chemical oxidation states would also cause an increase in H_2S adsorption capacity for the ZnO/rGO composite. From Fig. 4, representing C1s XPS data for ZnO/rGO composite, it is possible to determine the oxygen functional groups attached on the surface of rGO. The nature of those functional groups on the rGO surface are generally in agreement with previous studies [23,24]. The C1s spectra for ZnO/rGO composite can be fitted into four peaks for four different carbons: sp^2 carbon (284.6 eV), carbon in C–O bonds (286.3 eV), carbonyl carbon C═O (287.8 eV) and carboxylate carbon O—C═O (289.5 eV). The quantitative ratio of sp^2 carbon to carbon–oxygen groups is 0.96. This suggests that the rGO surface possesses significant amount of oxygen functional groups. Those oxygen functional

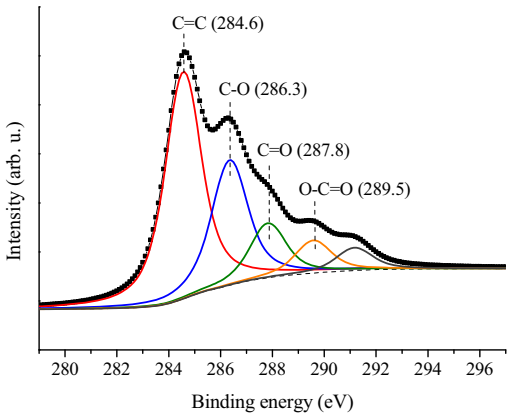

Fig. 4. C1s XPS for ZnO/rGO composite.

groups are chemically bonded with ZnO particles and modify the electrochemistry of ZnO.

From the Zn 2p XPS, the binding energy (BE) difference between the Zn 2p1/2 (1045.53 eV) and Zn 2p3/2 (1022.37 eV) was 23.16 eV for pure ZnO. The BE difference for ZnO/rGO was identical to 23.16 eV (1048.01 eV for Zn 2p1/2 and 1024.85 eV for Zn 2p3/2). This implies that the oxidation state of ZnO deposited on rGO surface is +2. In addition, a slight shift of BEs toward higher BE was observed when ZnO particles were loaded onto the rGO surface. This indicates that the interaction between ZnO and rGO is not only of physical nature but also of chemical nature. In order to investigate in more details the electrochemical states for Zinc, Zn 2p3/2 peaks for pure ZnO and ZnO/rGO composite were compared (Fig. 5).

The Zn 2p3/2 peak could be fitted by two major Zn peaks in the binding energy of ~1022 (Zn^I) and ~1023 eV (Zn^{II}), as shown in Fig. 6. The Zn^I phase represents the characteristic of Zn atoms in Zn–O bonds; the Zn^{II} phase is assigned to the Zn in the Zn–O bonds surrounded by oxygen vacancies implying that Zn atoms are not exactly occupied in the ZnO lattice [22,25]. It is clearly observed that the pure ZnO and ZnO/rGO composite possess different oxidation states, as shown in Fig. 6(a) and (d), respectively. The difference could be caused by the interaction between the ZnO and the oxygen-containing functional groups attached on the rGO surface. For pure ZnO, the area ratio of Zn^I to Zn^{II} is 2.21; and it becomes 1.13 for the ZnO/rGO composite. This suggests that for pure ZnO, Zn atoms are dominantly occupied in the ZnO lattice.

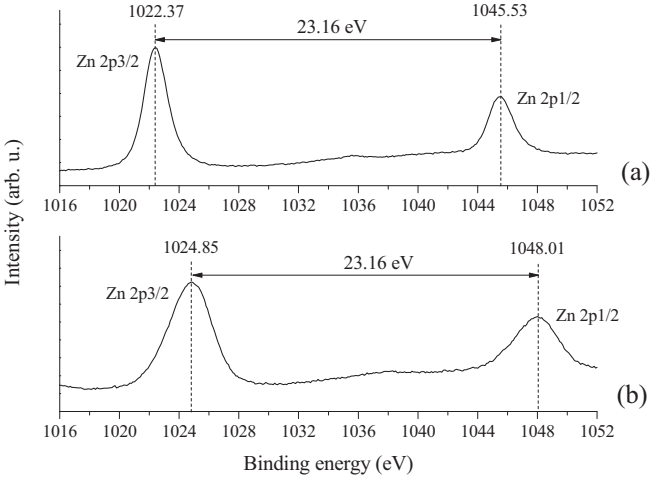

Fig. 5. Zn 2p XPS for (a) pure ZnO and (b) ZnO/rGO composite.

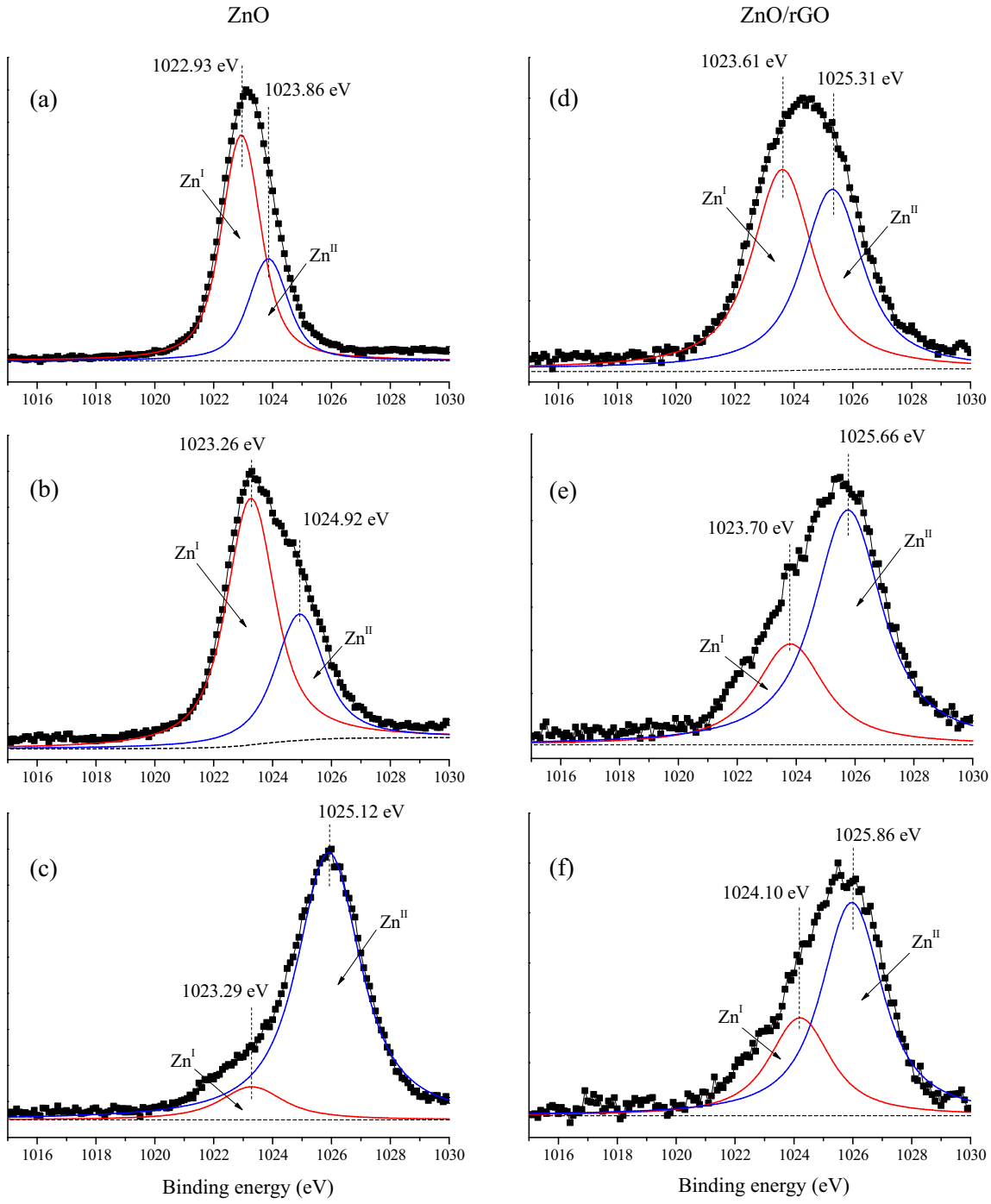

Fig. 6. Zn 2p3/2 spectra for ZnO (a) fresh, (b) after 1st regeneration and (c) after 5th regeneration; and ZnO/rGO (d) fresh, (e) after 1st regeneration and (f) after 8th regeneration.

However, when ZnO particles are attached onto the rGO surface, the chemistry of ZnO is modified due to the oxygen functional groups attached on the rGO surface. It could thus be inferred that when the oxygen functional groups are anchoring the metal ions during the synthesis process, the abundant amount of Zn ions are located at the oxygen vacancy sites. It is widely proposed that the dissociated H_2S ions (i.e. HS^- and S^{2-}) should be bonded with Zn^{2+} ions ([2,26]) for the adsorption process. The above XPS analysis suggests that the Zn^{II} phase (Zn ions which are not exactly located in the Zn–O lattice) is a preferred state than the Zn^{I} phase for H_2S adsorption. Therefore, critical roles of rGO for H_2S adsorption are not only dispersion of ZnO but also modifying the Zn oxidation states to a more preferable state. The preferable state implies that the Zn ions are located in the oxygen vacancy sites (not in the Zn–O lattice structure); and present as active Zn^{2+} ions, which are ready to connect with the dissociated H_2S molecules (i.e. HS^- or S^{2-}) leading to enhanced H_2S adsorption capacity about 5.4 times than that of pure ZnO. Therefore, this indicates that the Zn atoms at the oxygen vacancy sites play important roles for enhancing the H_2S adsorption capacity.

Fig. 6(a)–(c) present the chemical state of Zn in the case of pure ZnO for fresh, after 1st regeneration and after 5th regeneration,

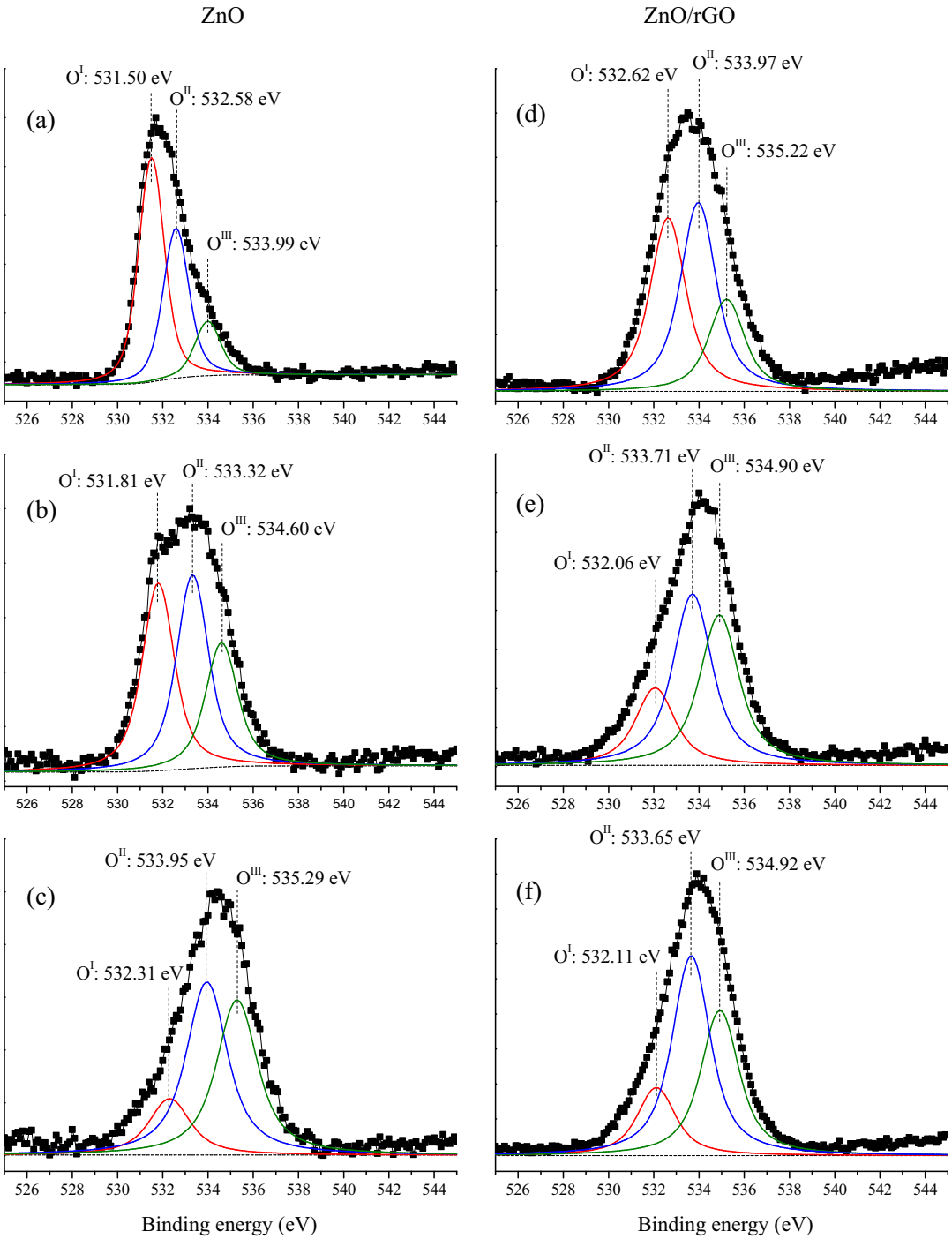

Fig. 7. O1s spectra for ZnO (a) fresh, (b) after 1st regeneration and (c) after 5th regeneration; and ZnO/rGO (d) fresh, (e) after 1st regeneration and (f) after 8th regeneration.

respectively. The ratios of Zn^{I}/Zn^{II} over the cycles were calculated as 2.21, 1.96 and 0.12, respectively. This implies that the Zn–O lattice matrix (representing Zn^{I}) was destroyed over the cycles since the dissociated HS^{-} or S^{2-} ions reacted with the zinc ions from the Zn–O lattice. In addition, the defects of ZnO (implying oxygen vacancy sites in ZnO lattice) increase the portion of heterogeneity of ZnO, and the oxygen vacancy is able to hinder the electron–hole recombination [27], which can increase the reactivity of H_2S adsorption. In this study, an oxygen source was not used for the regeneration process to prevent gasification of carbon support (rGO). Therefore, over the cycles, the Zn–O lattice structure was destroyed to produce ZnS structure, but no ZnO regeneration due to the lack of oxygen source. As a result, the Zn^{I}/Zn^{II} ratios for pure ZnO adsorbent decreased over the cycles.

Fig. 6(d)–(f) show the zinc chemical state changes over regeneration cycles for the ZnO/rGO composite sorbent. The initial ratio for ZnO/rGO was 1.13; after the first regeneration, the ratio decreased down to 0.44; and after the 8th cycle, the ratio was 0.45. After the first regeneration, the ratio was decreased since it could be expected that the Zn–O lattice structure was destroyed during the sulfidation process. However, interestingly, the Zn^{I}/Zn^{II} ratio after the first cycle and 8th cycle were similar. It implies that the chemical state of Zn in ZnO/rGO composite was not affected by high temperature regeneration condition (600 °C). This might

Table 1
Crystal structure for pure ZnO after H_2S exposure.

2θ	(hkl)	FWHM	a (nm)	c (nm)	Crystallite (nm)	d (Å)
31.76	(100)	0.2858	0.325		30.189	2.82
34.42	(002)	0.2946		0.521	29.486	2.60
36.26	(101)	0.3037			28.744	2.48
47.54	(102)	0.3714			24.412	1.91
56.60	(110)	0.3690			25.541	1.62

Table 2
Crystal structure for ZnO/rGO composite after H_2S exposure.

2θ	(hkl)	FWHM	a (nm)	c (nm)	Crystallite (nm)	d (Å)
31.62	100	0.3736	0.327		23.083	2.83
34.26	002	0.3383		0.523	25.664	2.62
36.12	101	0.4218			20.689	2.48
47.46	102	0.8204			11.048	1.91
56.38	110	0.5196			18.118	1.63

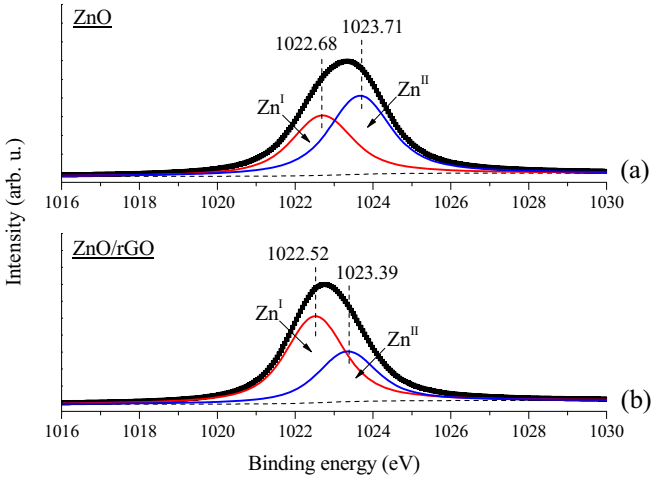

Fig. 8. After H_2S exposure Zn 2p3/2 XPS for (a) ZnO and (b) ZnO/rGO composite.

Table 3
Compositions of different chemical states for pure ZnO and ZnO/rGO composite.

Elements	Phases	Fresh		After H_2S exposure	
		ZnO (%)	ZnO/rGO (%)	ZnO (%)	ZnO/rGO (%)
Zn	I	84.5	38.6	43.3	63.3
	II	15.5	61.4	56.7	36.7
O	I	59.1	14.4	25.8	48.5
	II	26.7	39.3	52.1	38.0
	III	14.2	46.3	22.0	13.5
S	I			35.0	28.0
	II			65.0	35.7
	III				36.3

explain the critical role of the rGO. The stable chemical states of Zn caused by the presence of rGO over cycles can explain in part the stable adsorption capacity.

In order to explain the relationship between the lattice structure of ZnO and the H_2S adsorption capacity, the O1s XPS spectra is provided (see Fig. 7). It has been observed that the binding energy of O1s for ZnO/rGO was shifted toward higher binding energy than that of ZnO. This implies that the chemical bonding between the zinc and oxygen in ZnO/rGO was affected by the rGO which contains abundant oxygen functional groups [28,29]. Fig. 7 shows the

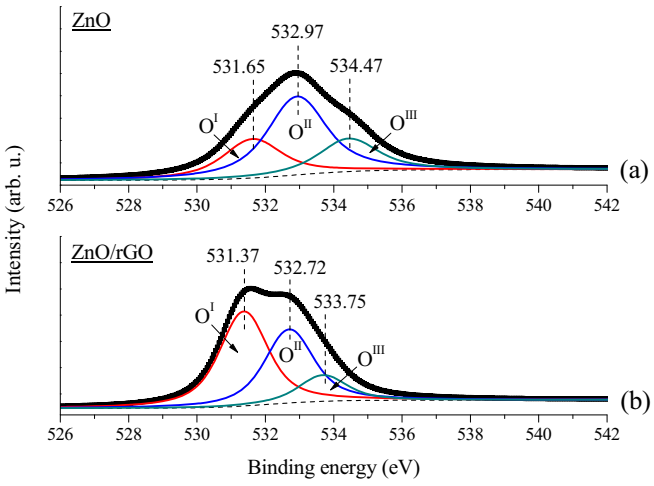

Fig. 9. After H_2S exposure O1s XPS for (a) ZnO and (b) ZnO/rGO composite.

oxygen chemical state changes over the regeneration cycles. The O1s peak can be divided into three groups as O^I, O^{II} and O^{III} [27]. The low binding energy peak (O^I) is attributed to the O^{2-} ions on the wurtzite ZnO lattice (~531 eV); the middle binding energy (O^{II}) is associated with O^{2-} ions in oxygen-deficient regions within the ZnO matrix (~532 eV); and the high binding energy (O^{III}) represents the loosely bound oxygen on the surface of ZnO (~534 eV) [30,31].

Fig. 7(a)–(c) show the changes of O1s sub-divided peaks from the fresh to 5th regenerations for pure ZnO. The ratio of O^I/O^{II} can represent the oxygen structure in the ZnO lattice. For the fresh ZnO, the ratio was 1.49 implying that most of oxygen O^{2-} ions are predominantly located in the Zn–O lattice. After the first sulfidation–regeneration cycle, the ratio decreased to 0.97; and further cycles (after 5th cycles) led to further decrease of this ratio to 0.32. These results support the fact that the sulfur ions (i.e. HS^- and S^{2-}) replace the oxygen ions in the Zn–O lattice; and produce Zn–S. In addition, over the cycles, the oxygen deficient sites were increased due to the lack of oxygen supplies during the regenerations.

Fig. 7(d)–(f) show that the oxygen chemical states in the Zn–O lattice in the ZnO/rGO composite had been modified due to the presence of rGO. The ratio of O^I/O^{II} for fresh ZnO/rGO sample was lower (0.92) than that for pure ZnO (1.49). It can be expected that the increase of the O^{II} fraction was caused by the oxygen functional groups on the rGO surface. The oxygen functional groups which are attached to the Zn–O lattice modified the oxygen chemical state in ZnO. After the first regeneration, the ratio for ZnO/rGO composite was decreased to 0.43; and after the 8th cycle, the ratio was further decreased to 0.39. However, the final ratios for ZnO/rGO (0.39 after 8 regenerations) and ZnO (0.32 after 5 regenerations) were not significantly different from each other after several regeneration cycles.

3.4. Characterizations of spent adsorbents

After the H_2S adsorption at 300 °C (in 750 ppm H_2S/N_2), several characterization techniques were conducted. The exposure to H_2S created new ZnS peaks located at $2\theta = 28.55°$ (111), 47.44° (220) and 56.39° (311) which are matched with JCPDS 77-2100 [32] and shown in Fig. 3(b) and (d). This confirms that ZnS is the product of the H_2S adsorption on ZnO. The intensity of the ZnS peak for pure ZnO is much weaker than the other ZnO peaks. However, for the ZnO/rGO composite, the ZnS peak is clearly visible. This indicates that the ZnO/rGO composite is more active for H_2S adsorption than pure ZnO. For both ZnO and ZnO/rGO composite, the ZnO

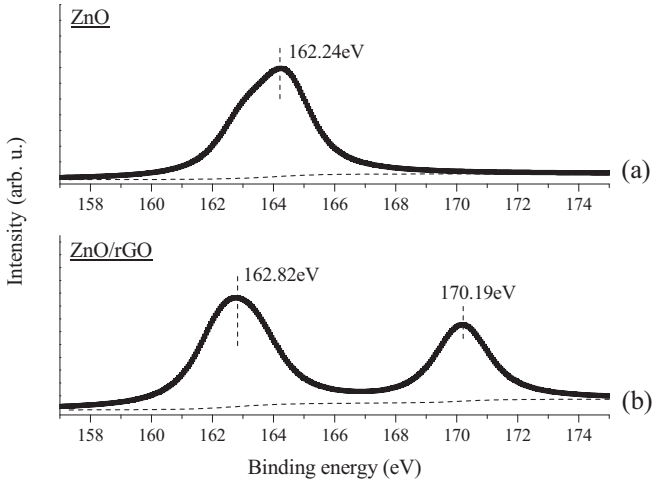

Fig. 10. S2p XPS for (a) ZnO and (b) ZnO/rGO composite after H_2S exposure.

peaks were still present, even after H_2S exposure. Detailed crystal structure analysis for ZnO and ZnO/rGO composite are listed in Tables 1 and 2. The characteristic peaks of ZnO are maintained for both samples after H_2S exposure. This suggests that the adsorption process did not change the crystal structure of ZnO. The lattice constants *a* and *c* for the remained ZnO were calculated as 0.325 and 0.521 nm, respectively for pure ZnO; and as 0.327 and 0.523 nm, respectively for the ZnO/rGO composite. Those lattice constants are almost identical to that of the fresh samples. In addition, *d*-spacing for ZnO and ZnO/rGO composite did not change either after the exposure. The FWHM value at (002) plane was 0.312° for fresh ZnO; and after H_2S exposure it was 0.295° for the spent ZnO. However, for ZnO/rGO composite, the FWHM value was 0.247° for fresh and 0.338° for the spent sample. This indicates that for pure ZnO, the FWHM values were not changed significantly; but, for ZnO/rGO composite, the FWHM values increased, implying that the crystallite size decreased. The grain sizes of pure ZnO at (002) plane were 27.825 nm (fresh) and 29.486 nm (spent); but for ZnO/rGO composite, the grain sizes were changed from 35.211 nm (fresh) to 25.664 nm (spent). In summary, for both ZnO and ZnO/rGO composite, the characteristics of ZnO particles were not affected even after H_2S exposure since the lattice constants (*a* and *c*) and *d*-spacing remained unchanged. However, the crystallite sizes (or grain size) were affected. For pure ZnO, the crystallite sizes did not change significantly, but for the ZnO/rGO composite, the crystallite sizes clearly decreased after H_2S exposure.

Fig. 8 shows the Zn 2p3/2 XPS data after H_2S exposure, and Table 3 presents the summary of the corresponding fractions of Zn, O and S in their various phases. After H_2S exposure, the fraction of Zn^{II} phase for pure ZnO decreased significantly (from 56.7% to 36.7%) implying that the zinc ions at the oxygen vacancy sites (Zn^{II}) participated during the adsorption process. For the ZnO/rGO composite, it was observed from the fresh sample that Zn^{2+} ions located near the oxygen vacancy sites were dominant (61.4%) because the rGO contains abundant oxygen functional groups on the surface. This suggests that the oxygen functional groups from the rGO provides Zn ions which are loosely bonded in Zn–O and located near the oxygen vacancy sites (Zn^{II}) for HS^- and S^{2-} ions. Therefore, those Zn^{2+} ions preferably reacted with sulfur ions and turned to ZnS.

As mentioned earlier, abundant O^{II} and O^{III} phases in ZnO/rGO composite had a critical role to enhance the H_2S adsorption capacity since those phases provide surface oxygen to H_2S molecules which can promote the dissociation of H_2S into HS^- and S^{2-}. Three major sub-peaks were also found after H_2S exposure (Fig. 9). For spent ZnO, O^{I} at 531.65 eV, O^{II} at 532.97 eV and O^{III} at 534.47 eV;

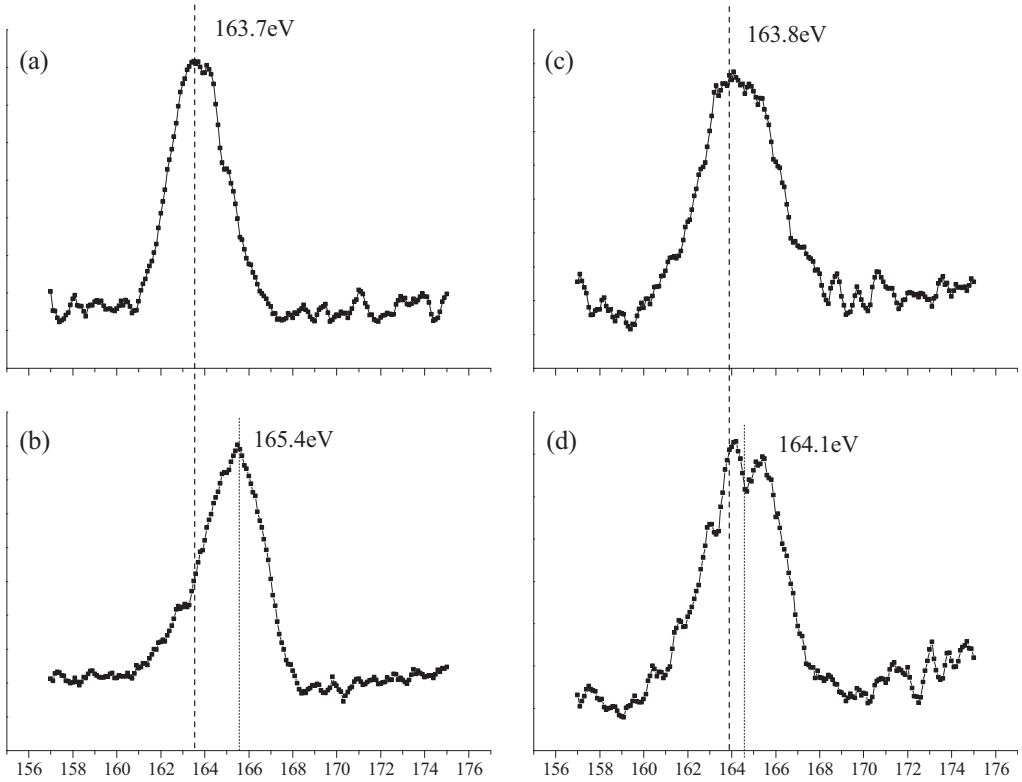

Fig. 11. S2p spectra for ZnO (a) after 1st regeneration, (b) after 5th regeneration; and for ZnO/rGO, (c) after 1st regeneration, (d) after 8th regeneration.

for spent ZnO/rGO composite, O^{I} at 531.37 eV, O^{II} at 532.72 eV and O^{III} at 533.75 eV were observed. The slight BE shift toward higher range from the fresh samples disappeared. The quantitative fraction for O^{I}, O^{II}, and O^{III} also changed (Table 3). For spent ZnO, the O^{I} phase (59.1% for fresh sample) decreased to 25.8% implying that oxygen in Zn–O lattice had participated dominantly in the adsorption process. After the adsorption process, most of the oxygen ions were in phase II (52.1% for O^{II}). However, oxygen ions in ZnO/rGO composite behaved differently. Most of oxygen ions located on the surface and oxygen vacancy sites participated in the adsorption. The portion of O^{III} from the fresh sample (46.3%) decreased to 13.5%. The O^{III} phase is also considered as oxygen ions originated from the oxygen functional groups on the rGO surface. This suggests that the rGO composite could provide chemically adsorbed moisture or loosely bonded oxygen ions to ZnO which are preferentially active with sulfur containing ions (HS^- and S^{2-}) for the adsorption.

Fig. 10 shows the XPS S2p spectra after the first H_2S adsorption. The presence of S2p spectra confirms the sulfidation of ZnO to ZnS. For pure ZnO, one S2p peak was observed at 162.24 eV which is assigned as S2p3/2, and this phase represents the sulfide S^{2-} ions in Zn–S [28,33]. For ZnO/rGO composite, one additional S2p peak at 170.19 eV was observed and it represents sulfate (SO_4^{2-}) [34,35]. The sulfate could originate from the loosely bonded oxygen ions (O^{II} and O^{III}) which are not located in the Zn–O lattice. Those oxygen ions located at the vacancy sites or surface should be able to contact with HS^- and S^{2-} ions easily and turn to sulfate. However, pure ZnO possesses oxygen ions in Zn–O lattice. Therefore, in order to react with sulfur ions, the Zn–O lattice should be destroyed to provide available Zn^{2+} and O^{2-} ions. This supports the fact that ZnO/rGO composite showed about fivefold higher H_2S adsorption capacity than that of pure ZnO.

Fig. 11 shows the S2p chemical state changes over regeneration cycles. Fig. 11(a) and (b) represent the changes on S2p for ZnO after 1st regeneration and 5th regeneration, respectively. It is seen that the binding energy (BE) shift to higher BE (+1.7 eV) over 5 cycles. This S2p BE shift implies that more positively charged sulfur atoms are present [36]. However, for ZnO/rGO composite shown in Fig. 11(c) and (d), relatively small S2p BE shift to higher BE (+0.3 eV) was observed even for longer regeneration cycles (8 cycles). This can explained that why the presence of rGO improves the regeneration ability from ZnS.

4. Conclusions

For hydrogen sulfide (H_2S) removal, the critical role of the rGO for active ZnO nano-particle dispersion has been investigated. Those oxygen functional groups attached on rGO surface were anchoring metal oxides, thus helping the dispersion of the active ZnO particles on the surface, resulting in preventing the aggregation effect which could allow for higher specific surface area of the active ZnO to H_2S gas. From H_2S breakthrough tests, it was confirmed that the ZnO/rGO composite showed almost 5.4 times higher ZnO utilization efficiency than the pure ZnO particle at 300 °C. Then, the H_2S adsorption capacity for pure ZnO decreased to almost zero after 5th cycles while that of ZnO/rGO composite maintained a capacity of 93.1 mg S/g ads (about 54% efficiency) over 8 cycles. It is proposed that rGO, possessing large amounts of oxygen functional groups, resisted the destruction of the ZnO lattice matrix over cycles.

Acknowledgments

This research was supported by the National Sciences and Engineering Research Council of Canada (NSERC); and by a Grant from Korea Institute of Energy Research (KIER) under Korea Research Council for Industrial Science and Technology, the Ministry of Knowledge and Economy, South Korea.

References

[1] J.A. Rodriguez, A. Maiti, Adsorption and decomposition of H_2S on MgO(100), NiMgO(100), and ZnO(0001) surfaces: a first-principles density functional study, J. Phys. Chem. B 104 (2000) 3630–3638.
[2] A. Samokhvalov, B.J. Tatarchuk, Characterization of active sites, determination of mechanisms of H_2S, COS and CS_2 sorption and regeneration of ZnO low-temperature sorbents: past, current and perspectives, Phys. Chem. Chem. Phys. 13 (2011) 3197–3209.
[3] C.L. Garcia, J.A. Lercher, Adsorption of hydrogen sulfide on ZSM 5 zeolites, J. Phys. Chem. 96 (1992) 2230–2235.
[4] H.G. Karge, R. János, Hydrogen sulfide adsorption on faujasite-type zeolites with systematically varied Si–Al ratios, J. Colloid Interface Sci. 64 (1978) 522–532.
[5] J.P. Wakker, A.W. Gerritsen, J.A. Moulijn, High temperature H_2S and COS removal with MnO and FeO on γ-Al_2O_3 acceptors, Ind. Eng. Chem. Res. 32 (1993) 139–149.
[6] T.-H. Ko, H. Chu, L.-K. Chaung, The sorption of hydrogen sulfide from hot syngas by metal oxides over supports, Chemosphere 58 (2005) 467–474.
[7] P. Dhage, A. Samokhvalov, D. Repala, E.C. Duin, M. Bowman, B.J. Tatarchuk, Copper-promoted ZnO/SiO_2 regenerable sorbents for the room temperature removal of H_2S from reformate gas streams, Ind. Eng. Chem. Res. 49 (2010) 8388–8396.
[8] M.V. Twigg, M.S. Spencer, Deactivation of copper metal catalysts for methanol decomposition, methanol steam reforming and methanol synthesis, Top. Catal. 22 (2003) 191–203.
[9] S. Lew, K. Jothimurugesan, M. Flytzani-Stephanopoulos, High-temperature H_2S removal from fuel gases by regenerable zinc oxide–titanium dioxide sorbents, Ind. Eng. Chem. Res. 28 (1989) 535–541.
[10] X.Y. Kong, Y. Ding, Z.L. Wang, Metal-semiconductor Zn–ZnO core–shell nanobelts and nanotubes, J. Phys. Chem. B 108 (2004) 570–574.
[11] M. Seredych, O. Mabayoje, T.J. Bandosz, Visible-light-enhanced interactions of hydrogen sulfide with composites of zinc (Oxy)hydroxide with graphite oxide and graphene, Langmuir 28 (2012) 1337–1346.
[12] O. Mabayoje, M. Seredych, T.J. Bandosz, Enhanced reactive adsorption of hydrogen sulfide on the composites of graphene/graphite oxide with copper (hydr)oxychlorides, ACS Appl. Mater. Interfaces 4 (2012) 3316–3324.
[13] O. Mabayoje, M. Seredych, T.J. Bandosz, Cobalt (hydr)oxide/graphite oxide composites: importance of surface chemical heterogeneity for reactive adsorption of hydrogen sulfide, J. Colloid Interface Sci. 378 (2012) 1–9.
[14] C. Xu, X. Wang, J. Zhu, X. Yang, L. Lu, Deposition of Co_3O_4 nanoparticles onto exfoliated graphite oxide sheets, J. Mater. Chem. 18 (2008) 5625–5629.
[15] I.V. Lightcap, T.H. Kosel, P.V. Kamat, Anchoring semiconductor and metal nanoparticles on a two-dimensional catalyst mat. Storing and shuttling electrons with reduced graphene oxide, Nano Lett. 10 (2010) 577–583.
[16] B. Adhikari, A. Biswas, A. Banerjee, Graphene oxide-based hydrogels to make metal nanoparticle-containing reduced graphene oxide-based functional hybrid hydrogels, ACS Appl. Mater. Interfaces 4 (2012) 5472–5482.
[17] M. Seredych, T.J. Bandosz, Reactive adsorption of hydrogen sulfide on graphite oxide/$Zr(OH)_4$ composites, Chem. Eng. J. 166 (2011) 1032–1038.
[18] X. Zhou, X. Huang, X. Qi, S. Wu, C. Xue, F.Y.C. Boey, Q. Yan, P. Chen, H. Zhang, In situ synthesis of metal nanoparticles on single-layer graphene oxide and reduced graphene oxide surfaces, J. Phys. Chem. C 113 (2009) 10842–10846.
[19] H.S. Song, M.G. Park, E. Croiset, Z. Chen, S.C. Nam, H.-J. Ryu, K.B. Yi, Effect of active zinc oxide dispersion on reduced graphite oxide for hydrogen sulfide adsorption at mid-temperature, Appl. Surf. Sci. 280 (2013) 360–365.
[20] H.S. Song, M.G. Park, S.J. Kwon, K.B. Yi, E. Croiset, Z. Chen, S.C. Nam, Hydrogen sulfide adsorption on nano-sized zinc oxide/reduced graphite oxide composite at ambient condition, Appl. Surf. Sci. 276 (2013) 646–652.
[21] H.S. Song, C.H. Ko, W. Ahn, B.J. Kim, E. Croiset, Z. Chen, S.C. Nam, Selective dibenzothiophene adsorption on graphene prepared using different methods, Ind. Eng. Chem. Res. 51 (2012) 10259–10264.
[22] P. Dhage, A. Samokhvalov, D. Repala, E.C. Duin, B.J. Tatarchuk, Regenerable Fe–Mn–ZnO/SiO_2 sorbents for room temperature removal of H_2S from fuel reformates: performance, active sites, operando studies, Phys. Chem. Chem. Phys. 13 (2011) 2179–2187.
[23] J. Xie, W.-T. Song, S.-Y. Liu, G.S. Cao, T. Zhu, X.B. Zhao, Self-assembly of $ZnFe_2O_4$/graphene hybrid and its application as high-performance anode material for Li-ion batteries, New J. Chem. 36 (2012) 2236–2241.
[24] S. Dubin, S. Gilje, K. Wang, V.C. Tung, K. Cha, A.S. Hall, J. Farrar, R. Varshneya, Y. Yang, R.B. Kaner, A one-step, solvothermal reduction method for producing reduced graphene oxide dispersions in organic solvents, ACS Nano 4 (2010) 3845–3852.
[25] G. Liu, Z.-H. Huang, F. Kang, Preparation of ZnO/SiO_2 gel composites and their performance of H_2S removal at room temperature, J. Hazard. Mater. 215–216 (2012) 166–172.
[26] D. Jiang, L. Su, L. Ma, N. Yao, X. Xu, H. Tang, X. Li, Cu–Zn–Al mixed metal oxides derived from hydroxycarbonate precursors for H_2S removal at low temperature, Appl. Surf. Sci. 256 (2010) 3216–3223.
[27] F.S. Omar, H.N. Ming, S.M. Hafiz, L.H. Ngee, Microwave synthesis of Zinc oxide/reduced graphene oxide hybrid for adsorption–photocatalysis application, Int. J. Photoenergy 2014 (2014) 176835.

[28] H. Ma, J. Han, Y. Fu, Y. Song, C. Yu, X. Dong, Synthesis of visible light responsive ZnO–ZnS/C photocatalyst by simple carbothermal reduction, Appl. Catal. B 102 (2011) 417–423.
[29] J. Wang, T. Tsuzuki, B. Tang, X. Hou, L. Sun, X. Wang, Reduced graphene oxide/ZnO composite: reusable adsorbent for pollutant management, ACS Appl. Mater. Interfaces 4 (2012) 3084–3090.
[30] S. Aksoy, Y. Caglar, S. Ilican, M. Caglar, Sol–gel derived Li–Mg co-doped ZnO films: preparation and characterization via XRD, XPS, FESEM, J. Alloy. Compd. 512 (2012) 171–178.
[31] A. Prakash, S.K. Misra, D. Bahadur, The role of reduced graphene oxide capping on defect induced ferromagnetism of ZnO nanorods, Nanotechnology 24 (2013) 095705.
[32] A.M. Palve, S.S. Garje, A facile synthesis of ZnS nanocrystallites by pyrolysis of single molecule precursors, Zn (cinnamtscz)$_2$ and $ZnCl_2$ (cinnamtsczH)$_2$, Bull. Mater. Sci. 34 (2011) 667–671.
[33] L. Fen, Y. Bo, Z. Jie, J. Anxi, S. Chunhong, K. Xiangji, W. Xin, Study on dsulfurization efficiency and products of Ce-doped nanosized ZnO desulfurizer at ambient temperature, J. Rare Earths 25 (2007) 306–310.
[34] J.E. Thomas, W.M. Skinner, R.S.C. Smart, A comparison of the dissolution behavior of troilite with other iron(II) sulfides; implications of structure, Geochim. Cosmochim. Acta 67 (2003) 831–843.
[35] Z.-H. Huang, G. Liu, F. Kang, Glucose-promoted Zn-based metal–organic framework/graphene oxide composites for hydrogen sulfide removal, ACS Appl. Mater. Interfaces 4 (2012) 4942–4947.
[36] S. Fleutot, J.C. Dupin, I. Baraille, C. Forano, G. Renaudin, F. Leroux, D. Gonbeau, H. Martinez, A new route for local probing of inner interactions within a layered double hydroxide/benzene derivative hybrid material, Phys. Chem. Chem. Phys. 11 (2009) 3554–3565.